

Efficient Multisensory Barrier for Obstacle Detection on Railways

J. Jesús García, *Member, IEEE*, Jesús Ureña, *Member, IEEE*, Álvaro Hernández, *Member, IEEE*, Manuel Mazo, *Member, IEEE*, José Antonio Jiménez, Fernando J. Álvarez, Carlos De Marziani, Ana Jiménez, M. Jesús Díaz, Cristina Losada, and Enrique García

Abstract—On current railway systems, it is becoming ever more necessary to install safety elements to avoid accidents. One of the causes that can provoke serious accidents is the existence of obstacles on the tracks, either fixed or mobile. In this paper, a multisensory system that can inform the monitoring system about the existence of obstacles is proposed. The system for obstacle detection consists of two emitting and receiving barriers, which are placed on opposing sides of the railway, respectively, and use infrared and ultrasonic sensors, thus establishing different optical and acoustic links between them. The interruption of one or several links should produce an alarm. However, even without the existence of objects, degradation of links could occur due to atmospheric attenuation, solar radiation, etc., also producing an activation of the alarm system. Since detection is based on the lack of radiation in the detectors, the use of complementary sensors for the same task is justified. Since the minimum size of an object for which an alarm is required to be generated is $50 \times 50 \times 50$ cm, in some situations, several links are interrupted; however, alarms should not be generated. Typical cases are the flight of leaves or the movement of small animals in the scanned area. To avoid alarm activation in such situations, this paper proposes the combined use of diverse techniques of data fusion, based on fuzzy logic and the Dempster–Shafer theory of evidence, to validate the existence of objects, providing a highly reliable detection system.

Index Terms—Data fusion, infrared (IR) and ultrasonic (US) sensors, railway safety, sensor-emission encoding, validation of obstacle detection.

Manuscript received July 23, 2008; revised April 28, 2009, October 5, 2009, and February 1, 2010; accepted April 23, 2010. Date of publication June 28, 2010; date of current version September 3, 2010. This work was supported by the Spanish Ministry of Education and Science under Project TIN2006-14896-C02-01, the Ministry of Public Works through the Project 70025/T05, and the University of Alcalá through Project CCG06-UAH/DPI-0748. The Associate Editor for this paper was N. Zheng.

J. J. García, J. Ureña, Á. Hernández, M. Mazo, J. A. Jiménez, A. Jiménez, M. J. Díaz, C. Losada, and E. García are with the Department of Electronics, University of Alcalá, 28805 Madrid, Spain (e-mail: jesus@depeca.uah.es; urena@depeca.uah.es; alvaro@depeca.uah.es; mazo@depeca.uah.es; jimenez@depeca.uah.es; ajimenez@depeca.uah.es; mjesus@depeca.uah.es; losada@depeca.uah.es; enrique.garcia@depeca.uah.es).

F. J. Álvarez is with the Department of Electrical Engineering, Electronics, and Automatics, University of Extremadura, 06071 Badajoz, Spain (e-mail: fafranco@unex.es).

C. De Marziani is with the Department of Electronics, National University of Patagonia San Juan Bosco, 9005 Comodoro-Rivadavia, Argentina (e-mail: marziani@unpata.edu.ar).

Color versions of one or more of the figures in this paper are available online at <http://ieeexplore.ieee.org>.

Digital Object Identifier 10.1109/TITS.2010.2052101

I. INTRODUCTION

IN ALL transport systems, particularly in the case of railways, *safety* and *reliability* are highly considered [1]. Because of the constant need to improve railway safety, several European projects [2] are carrying out research into whatever circumstances that exist that may pose a threat to railway safety. One such circumstance has received particular attention in the case of some of these projects [3]: *the existence of objects on the tracks*.

On nonhigh-speed lines (standard lines), there exist critical areas where it is necessary to detect the presence of obstacles: the level or grade crossings. A comparatively high amount of dedicated sensory systems has been installed in areas at or near level crossings to prevent collisions between trains and vehicles (in [4], there is recent analysis about the phenomena that may cause collisions at level crossings). On high-speed lines, there are no level crossings, but zones close to bridges or tunnels are considered to be quite critical since objects can fall onto the tracks. This can be caused by the fall of a vehicle, or a material being transported by a vehicle, onto the line. Landslides can also happen at the entrances and exits of tunnels. In these critical areas, if there is a system to detect the presence of obstacles [5]–[8], railway traffic can be halted, and possible accidents can be avoided. These systems sometimes generate false alarms, thus creating financial losses whenever the system detects an obstacle that does not actually exist. To avoid the generation of false alarms, it has become necessary to increase the reliability of the detection system. Reliability is highly influenced by the design of the sensor used, the conditions in which the sensor is working, and the signal processing that is carried out by the system. This paper focuses on one of such systems to detect obstacles on high-speed lines in a reliable way.

In some adverse conditions of a railway environment, there are often marked differences in the performance of various types of sensors, as each type used will have its own inherent weaknesses and limitations. For example, weather conditions (rain, fog, etc.) are a problem when using cameras; optical sensors produce false alarms due to solar radiation or weather conditions (in [9], a full study about the degradation of optical signals can be found); the same problem is found using ultrasonic (US) sensors if the system is working in a turbulent atmosphere [10], [11] (e.g., when wind speeds are high or fluctuating).

Due to the fact that the ideal sensor does not exist [12]–[14], in this paper, a multisensory system is proposed so that the

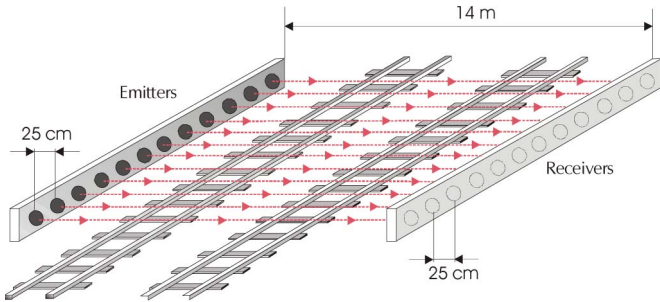


Fig. 1. Scheme of the multisensory barrier.

drawbacks of using any particular type of sensor are outweighed by the performance characteristics of the other types of sensors that are used in certain given sets of circumstances. In this particular case, the proposal is based on a multisensory barrier consisting of *IR* and *US* sensors. The proposed system meets the requirements of Spanish Railway Regulations for obstacle detection on high-speed lines [15] (it is important to point out that the requirements were specified only for an *IR* barrier). Apart from the use of a multisensory barrier, there are other reasons that will improve the reliability of the detection system. First, a robust codification scheme based on mutually orthogonal complementary sets of sequences is proposed. It simultaneously provides multiple emissions and multiple receptions, avoids interference among the emissions, and can function with a low signal-to-noise ratio. Second, the use of fuzzy logic to combine the information given by the two sensors (*IR* and *US*) is proposed. Finally, the fusion of this information by means of the Dempster–Shafer evidential theory [16] is proposed to obtain a certainty value for the existence of objects (greater than $50 \times 50 \times 50$ cm), which may pose a risk to railway traffic.

According to the proposal, this paper is organized as follows: Section II introduces the designed sensory system. Section III deals with the process of validating the existence of obstacles, based on data-fusion techniques. Section IV describes some real tests. Finally, some conclusions are discussed in Section V.

II. DESIGNED SENSORY SYSTEM

A. Detection System

The designed sensory system is composed of two multisensory barriers, i.e., one emitting and the other receiving, which are placed at both sides of the railway, as shown in Fig. 1. The most important features and performance characteristics of the sensory system are detailed in [15] and [17]. In summary, the minimum dimensions of the object to be detected are $50 \times 50 \times 50$ cm, whereas the distance between contiguous transducers is 25 cm. As a result, if an object with minimum dimensions is in the scanned area, at least two links are interrupted. The distance between emitters and receivers is 14 m, given the width of the railway line, although the distance between emitters and receivers may be sometimes greater. According to Spanish Railway Regulations [15], the required scan time is 500 ms, and if an obstacle is inside the detection area for more than 3 s, an alarm must be generated. Fig. 2 shows a proposal for an obstacle-detection system. It

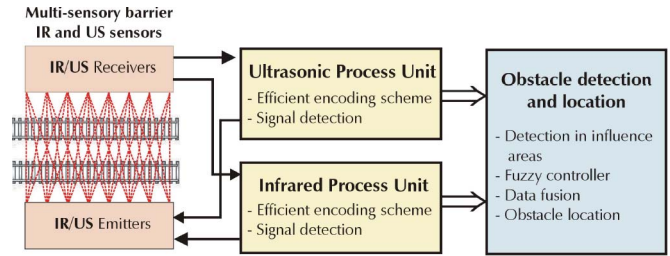


Fig. 2. Block diagram of the proposed detection system.

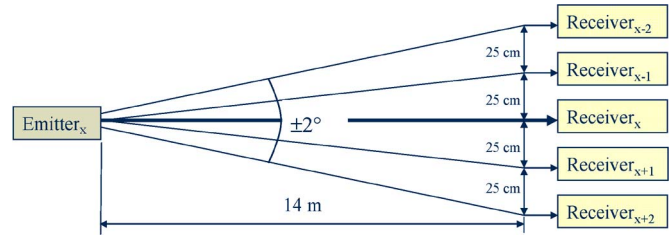


Fig. 3. Emission aperture for an *IR* emitter.

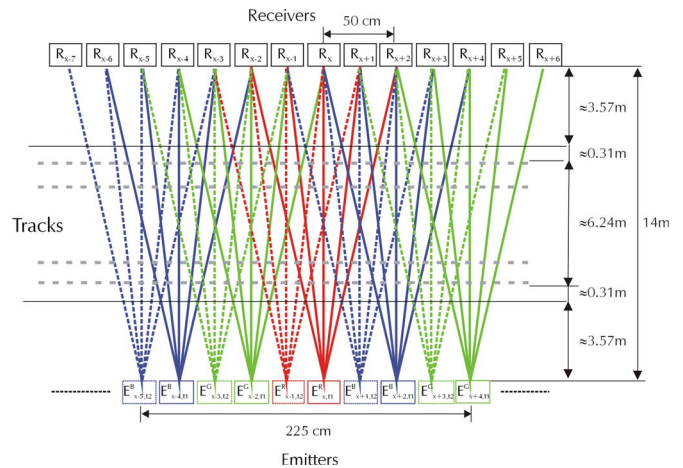


Fig. 4. Links at a segment of 2.25 m.

is divided into three processing levels: 1) the sensory modules (the multisensory barrier); 2) the individual process units; and 3) an integration module for obstacle detection and location.

Due to the aperture angle of the emitters that are either *IR* or *US*, every emission reaches a group of receivers. This allows multiple links to be established in the sensory system, apart from those on the axial axis shown in Fig. 1. For example, an *IR* emitter with an aperture angle of $\pm 2^\circ$, at a distance of 14 m from a receiving barrier, can send emissions to up to five receivers, thus establishing five connections per emitter, as depicted in Fig. 3. Furthermore, five separate emissions reach every receiver. In the case of *US* emitters, the aperture angle is higher; however, to have the same links and similar information in both barriers, only five links are taken into account.

Fig. 4 shows the established links for a segment of ten emitters (2.25 m). The proposed structure has several improvements, taking into account the requirements. On one hand, if there exists a minimum-dimension obstacle in the supervised area, at least ten links are interrupted. In [15], only two interrupted

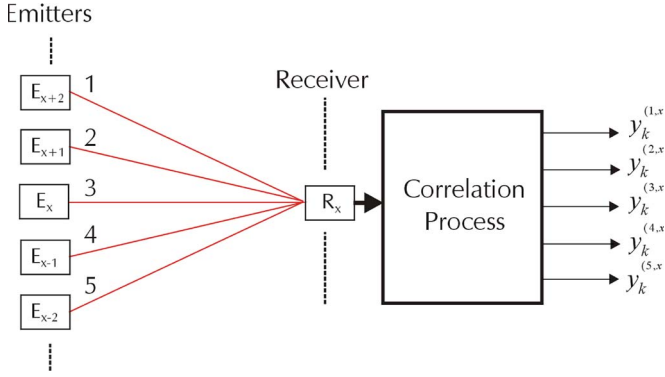


Fig. 5. Block diagram of the detection process.

links are required to detect the obstacle. On the other hand, due to the fact that the detection is based on link interruptions, if a sensor is not working, it could be mistaken for obstacle detection. Nevertheless, the number of interrupted links allows the system to distinguish the presence of an obstacle from a sensor that is out of order, this being of particular advantage for maintenance tasks. Finally, using this structure, the system can detect the location of obstacles [18] within two main zones: *on the tracks or outside of the tracks*.

B. Emission Encoding

Since a multimode operation is carried out in the barrier [19] (simultaneous multiemission and multireception), it is necessary to encode every emission to avoid interferences among the different emissions and to discriminate them at the receiving block. For that reason, mutually orthogonal complementary sets of sequences have been used [20]–[22]. More details about the encoding scheme and the adaptation of the different sensors can be found in [17].

In Fig. 4, every emitter uses a different code (shown by different levels of gray in the diagram). The detection of the different emissions is carried out by means of a correlation process, where the output of every receiver (either *IR* or *US*) provides five measurements, corresponding to the correlation values obtained for every link, as Fig. 5 shows. Due to the fact that the emitters transmit periodically, the correlation output obtained for every link is a periodic signal as shown by

$$y_k^{(j,x)} = G \cdot \theta_k \cdot \sum_{i=0}^{i=\infty} \delta[k - i \cdot T] + \phi_{n,k} \quad (1)$$

where G is the process gain, according to the encoding scheme [17]; T is the emission period (around 100 ms); θ_k represents atmospheric and lateral attenuation (lateral attenuation depends on the sensor emission pattern [17]); $\phi_{n,k}$ is the noise component after the correlation; x is the position of the receiver in the barrier; and $j \in \{1, 2, 3, 4, 5\}$ represents every link established in a receiver, as shown in Fig. 5. The index k represents the time instant when data are captured.

According to Fig. 5, the output of every receiver can be represented as a vector $\mathbf{y}_k^{(x)}$ of five measurements, as shown by

$$\mathbf{y}_k^{(x)} = \begin{bmatrix} y_k^{(1,x)} & y_k^{(2,x)} & y_k^{(3,x)} & y_k^{(4,x)} & y_k^{(5,x)} \end{bmatrix}^T \quad (2)$$

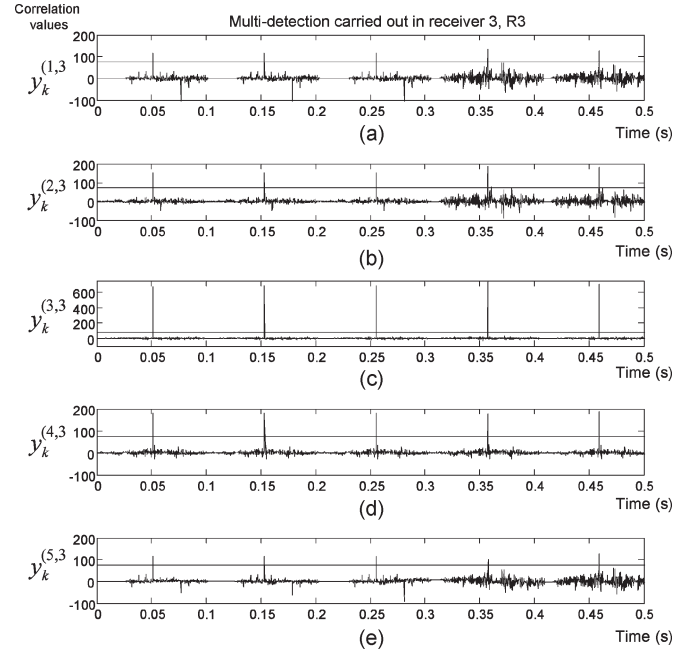


Fig. 6. Real correlation outputs obtained in an *IR* receiver when the links are not interrupted.

where x is the position of the receiver in the barrier, and k means the time instant. Every component of vector $\mathbf{y}_k^{(x)}$ is represented in (1).

Fig. 6 shows the multidetection carried out in an *IR* receiver in the absence of obstacles. The amplitude differences depend on the lateral deviations between emitters and the receiver (see Figs. 3 and 4); therefore, the maximum correlation output is provided by the emitter that is placed in the axial axis (note the axis scales).

In the following, the matrix \mathbf{Y}_k contains the correlation output of all the links in one of the barriers (*IR* or *US*):

$$\mathbf{Y}_k = \begin{bmatrix} y_k^{(1,1)} & \cdots & y_k^{(1,x)} & \cdots & y_k^{(1,X)} \\ y_k^{(2,1)} & \cdots & y_k^{(2,x)} & \cdots & y_k^{(2,X)} \\ y_k^{(3,1)} & \cdots & y_k^{(3,x)} & \cdots & y_k^{(3,X)} \\ y_k^{(4,1)} & \cdots & y_k^{(4,x)} & \cdots & y_k^{(4,X)} \\ y_k^{(5,1)} & \cdots & y_k^{(5,x)} & \cdots & y_k^{(5,X)} \end{bmatrix}_{5 \times X} \quad (3)$$

Every column of matrix \mathbf{Y}_k is the vector shown in (2), with X as the number of receivers in the barrier.

To evaluate if an established link j in the receiver x is interrupted, the correlation value $y_k^{(j,x)}$ should be less than a determined detection threshold T_H . However, even when the tracks are free of obstacles, the correlation value could be lower than the threshold due to the channel degradation (produced by weather conditions or solar radiation [23], [24]), and consequently, false alarms would be produced. As was shown in [18], false alarms can be reduced using a dynamic threshold $T_{H,k}^{(j,x)}$ that is dynamically adapted by considering meteorology and solar interference.

The generation of the dynamic threshold is based on the optimal estimation of the correlation output. Several optimal estimation techniques have been evaluated to generate the dynamic threshold: polynomial interpolation of degree 1 [18],

the Kalman filter (KF), and the H_∞ filter [19]. Polynomial interpolation did not completely reduce false alarms, and some limitations were found with the KF: It assumes that the statistical noise of the channel is known, and it minimizes the average estimation error. In [19], false alarms were generated when the noise was not zero mean, and its covariance matrix was unknown. To avoid this situation, the use of the H_∞ filter (also known as the *minimax* filter [25], [26]) was proposed for two main reasons: The detection system is based on US and IR technology, and it is difficult to characterize the channel noise; furthermore, the *minimax* filter minimizes the worst case of the estimation error (and not only the average as KF does; in [27], some examples are shown that demonstrate the advantages of H_∞ estimators in comparison with l_2 solutions). The second reason is very important considering the relationship between the transport safety and the correct detection of obstacles on the tracks. In [19], it was shown that the H_∞ filter properly works (without generating false alarms) with low signal-to-noise ratios (-6 dB) and even under bad weather conditions.

In this paper, the H_∞ filter gives an estimate $\hat{y}_k^{(j,x)}$ of the correlation value $y_k^{(j,x)}$ for every link j in every receiver x at every time instant, establishing the threshold at time instant k . The threshold at time instant k is determined to be half of the estimation at time instant $k - 1$ because it is not expected that the correlation value can decrease 50% due to channel degradation during a sampling time. However, to avoid false alarms, it is necessary to set a minimum threshold $T_{H-\min}$ according to the encoding scheme and the expected noise. As shown in Section IV, the minimum threshold has been determined experimentally, fixing it at 10% of the maximum expected correlation output G . The following equation shows how the dynamic threshold is generated:

$$T_{H,k}^{(j,x)} = \max \left(\frac{\hat{y}_{k-1}^{(j,x)}}{2}, T_{H-\min} \right). \quad (4)$$

Finally, an output $z_k^{(j,x)}$ corresponding to its state, i.e., *on* or *off*, is generated for every link, as shown in the following:

$$z_k^{(j,x)} = \begin{cases} 1 & \text{if } \hat{y}_k^{(j,x)} \geq T_{H,k}^{(j,x)} \\ 0 & \text{if } \hat{y}_k^{(j,x)} < T_{H,k}^{(j,x)}. \end{cases} \quad (5)$$

As in (3), two matrices \mathbf{Z}_k are obtained (one per barrier), representing the state of all the links (1, *on*; 0, *off*). Fig. 7 depicts the diagram block of a receiver that is tuned to a generic code considering the described process.

As concluded in (4), the threshold will be adapted to the slow changes of the channel produced by weather conditions or solar radiation. In contrast, an obstacle will generate a fast change of the channel, causing a lack of signal in the receiver, and, consequently, a low correlation value. As shown in [18] and [19], this strategy reduces false alarms due to the channel degradation.

III. OBJECT VALIDATION

In a railway environment, typical situations that can generate a false alarm must be identified. Although the occurrence of

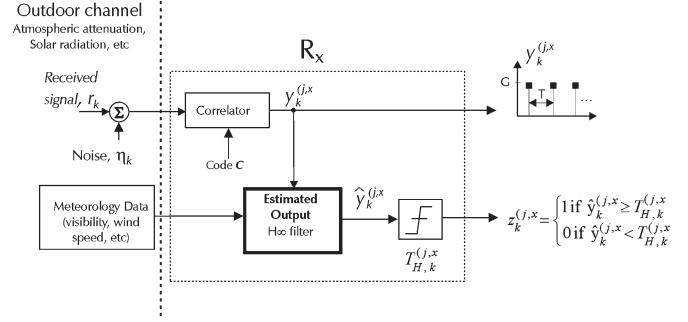


Fig. 7. Block diagram of a receiver R_x tuned to a generic code C .

false alarms has been notably reduced by using the dynamic threshold in the detection stage, it is still possible for some receivers not to detect emissions because a small object (moving leaves, small animals, etc.) has temporarily interrupted the link, or because weather conditions are severe, or simply because the corresponding emitter is damaged. These situations should not cause alarm activations.

The use of the two barriers to sense the same variable is justified to avoid some of the aforementioned problems so that the disadvantages of using any particular type of sensor are outweighed by the performance characteristics of the other types of sensors that are used in some circumstances. For example, solar radiation affects the IR barrier but not the US barrier, and US sensors have difficulties in a turbulent atmosphere, which is not the case for IR sensors over short distances. The objective then becomes how to integrate information received from the two barriers to detect the existence of objects larger than $50 \times 50 \times 50$ cm.

In the detection, two pieces of information must be present in every sensor output [28]: 1) the detection itself, i.e., the barriers provide this information in matrices \mathbf{Y}_k and \mathbf{Z}_k ; and 2) how well or with what confidence the sensor has been able to detect an object. For the latter, it is necessary to combine data from different sources, taking into account external variables such as weather conditions or sensor degradation. For the IR barrier, weather conditions can be modeled by considering *visibility* [23], [24]. There is a direct relation between visibility and atmospheric attenuation. For the US barrier, the main factor that can influence its performance is the level of turbulence, and to assess the effect of such turbulence, it is necessary to measure the wind speed [10]. It is also worth noting that the failure of just one individual link may be considered insignificant since if a dangerous object exists, at least ten links from each barrier will be interrupted, as was described in Section II. In summary, it is necessary to consider the two sensory barriers and the spatial redundancy existing at each barrier.

Considering the above remarks, the data fusion has been carried out at three levels. First, the detection area for each barrier has been divided into 25-cm-wide influence areas according to the receivers; therefore, if a dangerous object exists, it is detected in two consecutive influence areas. The result of this level is a measurement of the certainty of existence of objects in every influence area. Second, a fuzzy controller (the fuzzy controller theory can be found in [29]) has been included to weigh up the certainty of existence of objects in every influence area, taking into account the information given by the two

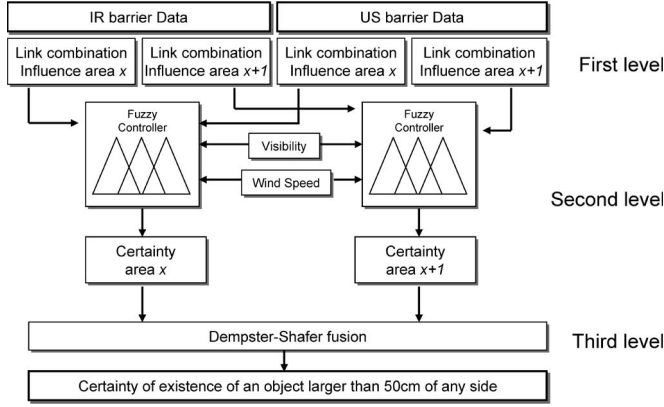


Fig. 8. Data-fusion architecture for two consecutive influence areas.

barriers and the visibility and wind-speed values. As a result, by fusing the information from the two barriers, a final value for the certainty of existence of objects in every influence area can be obtained. Finally, values for the certainty of the existence of objects belonging to two consecutive influence areas have been fused by means of the Dempster–Shafer evidential theory [28], [30] to obtain a final value for the certainty of existence of objects larger than $50 \times 50 \times 50$ cm. Fig. 8 shows the data fusion architecture carried out for two consecutive influence areas.

A. First Level. The Certainty of Existence of Objects in the Influence Area $A_{(x)}$

Fig. 9 shows the division of the detection area into influence areas (similar for both barriers). The influence area of the receiver R_x is represented by $A_{(x)}$. After the analysis of the influence area, a value for the certainty of existence of objects is obtained and is represented by $c_{A_{(x)}} \in [0, 1]$.

As Fig. 9 shows, which is more detailed in Fig. 10, there exist 11 links for every influence area that have been established between five emitters and five receivers. Note that these links cross several areas, except for the link between the emitter x and the receiver x , which only exists inside the area $A_{(x)}$. Assuming that a link belonging to area $A_{(x)}$ is interrupted by an object, the probability of the object to be in the area $A_{(x)}$ depends on the percentage of the range of the link that is placed in such an area. For the link between emitter x and receiver x (link $l_{x,x}$), the probability is 1; however, for the rest, it is 0.5 or 0.25. Table I shows the probability $\rho_{e,r}$ for every link inside a detection area. Subindexes e and r denote the x position of the emitter and the receiver, respectively.

To determine if a link is interrupted, it is only necessary to evaluate the state (*on*, *off*) of the corresponding element in the matrix \mathbf{Z}_k . Due to the fact that the channel degradation can generate a lack of signal in the detector, this situation can be mistaken for the existence of an object. For this reason, if, at any k instant, $z_k^{(j,x)}$ was zero—existence of an obstacle—but a high-level channel degradation occurred at the $k - 1$ instant, it would be very unlikely that the lack of signal was produced by an object. Therefore, to conclude if a link is interrupted by an object, in addition to the correlation value, it is necessary to consider the link degradation.

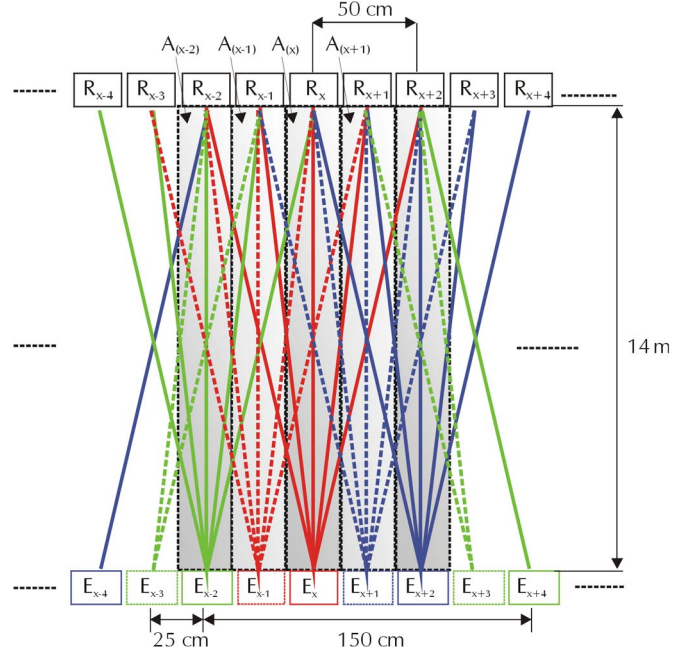


Fig. 9. Influence areas.

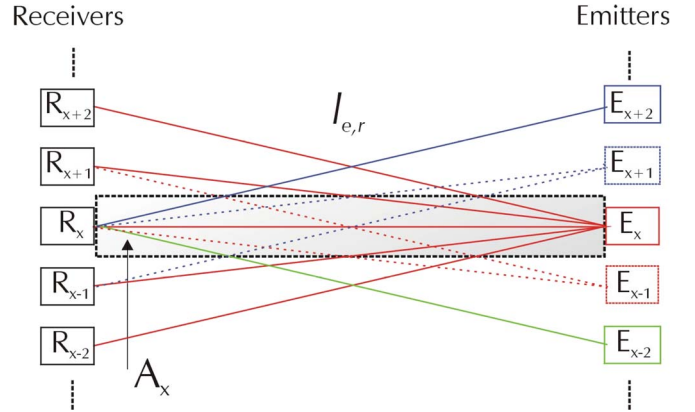


Fig. 10. Links for the influence area.

TABLE I
PROBABILITY OF AN OBJECT INTERRUPTING A LINK IN THE AREA $A_{(x)}$

Index i	$l_{e,r}$	$\rho_{e,r}$	Index i	$l_{e,r}$	$\rho_{e,r}$
-5	$l_{x,x-2}$	0.25	1	$l_{x+1,x}$	0.5
-4	$l_{x,x-1}$	0.5	2	$l_{x+2,x}$	0.25
-3	$l_{x+1,x-1}$	0.5	3	$l_{x-1,x+1}$	0.5
-2	$l_{x-2,x}$	0.25	4	$l_{x,x+1}$	0.5
-1	$l_{x-1,x}$	0.5	5	$l_{x,x+2}$	0.25
0	$l_{x,x}$	1			

Regarding this, assuming that a link is interrupted ($z_k^{(j,x)} = 0$), the certainty of interruption of a link ($l_{e,r}$) by an object between the emitter e and the receiver r is given as follows:

$$\begin{aligned} \sigma_{e,r} &= \alpha_{e,r} \cdot \rho_{e,r} \text{ if the link } l_{e,r} \text{ is interrupted (off)} \\ \sigma_{e,r} &= 0 \text{ if the link } l_{e,r} \text{ is not interrupted (on)} \end{aligned} \quad (6)$$

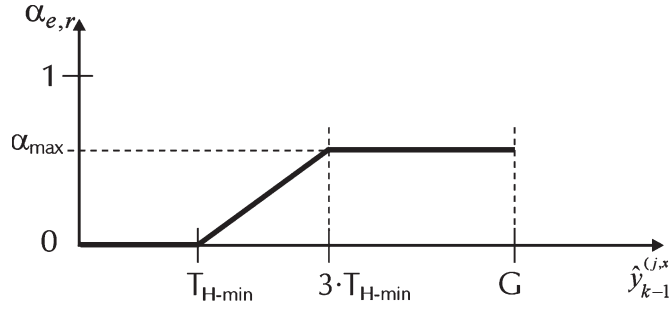


Fig. 11. Calculation of $\alpha_{e,r}$.

where $\alpha_{e,r}$ is the channel degradation before the interruption of the link $l_{e,r}$, and $\rho_{e,r}$ is the probability that the object is inside the area $A(x)$. The certainty $\sigma_{e,r}$ gives a measure about the degree of confidence about the state of the link that is provided by the sensory system. Due to the fact that the parameter $\sigma_{e,r}$ is considered only if the link $l_{e,r}$ is interrupted, in the case when the link is not interrupted (the corresponding $z_k^{(j,x)} = 1$), $\sigma_{e,r}$ is fixed at 0. The value of $\alpha_{e,r}$ is empirically computed according to Fig. 11.

In Fig. 11, $\alpha_{max} = 0.5$, T_{H-min} is the minimum threshold, G is the process gain [see (2)], and $\hat{y}_{k-1}^{(j,x)}$ is the estimate of the correlation carried out by the H_∞ filter at the $k - 1$ instant (before the interruption of the link). This estimate can be considered as a channel-degradation measurement, and it corresponds to the link between the emitter e and the receiver r (the lower the estimate of the correlation before the interruption of the link, the more degraded the channel). Experimental results show that if weather conditions are good, the correlation values obtained are always higher than $3 \cdot T_{H-min}$. Note that the maximum value of $\sigma_{e,r}$ has been fixed at 0.5.

After obtaining $\sigma_{e,r}$, the value for the certainty of the existence of obstacles in the area $A(x)$ is computed by considering the 11 links. If it is assumed that the probability of the link $l_{e,r}$ being interrupted by an object inside the area $A(x)$ is $\sigma_{e,r}$, then $c_{A(x)}$ is obtained as the union probability of independent events, as shown by the following:

$$\begin{aligned}
 P(l) &= 0 \\
 \text{for } i &= -5i \leq 5i + P(l_i \cup l) \\
 &= P(l_i) + P(l) - P(l_i) \cdot P(l) = P(l_i \cup l) \\
 \text{endfor} \\
 c_{A(x)} &= P(l). \tag{7}
 \end{aligned}$$

In (7), for convenience, the probability of every link is represented by $P(l_i)$, and i defines every link according to the assignment done in Table I.

Due to the fact that the maximum value of $\sigma_{e,r}$ is 0.5, it is important to remark that if the number of interrupted links in a barrier provides a value for the corresponding $c_{A(x)} > 0.5$ (it means that several links are interrupted), then it is possible that an object exists in the area $A(x)$.

B. Second Level. Fuzzy Controller

After the certainties of existence of objects for every zone and each barrier are available, it is necessary to combine them to have only one certainty value for every zone.

Fuzzy systems allow complex semantic reasoning to be easily included into the fusion system. Fuzzy logic introduces a concept of partial truth values that lie in between “completely true” and “completely false.” The central concept of fuzzy logic is the *membership* function, which numerically represents the degree of belonging of an element to a set. An element can be a member of a set at a certain degree and be a member of a different set at the same time. Therefore, the common-sense expression (e.g., give less confidence to US when the wind is fast) is naturally included in the fuzzy system as a knowledge rule over fuzzy sets.

To fairly combine the information of both barriers, it is strictly necessary to include weather conditions that affect the confidence level given by any of the barriers. As a result, the fuzzy reasoning has to be able to distinguish the situations of the presence of an obstacle from those of the degradation of the link due to environmental causes. These two situations cannot be detected by the barriers themselves in the previous steps. The proposal is to use a *Mamdani* fuzzy controller [31], which models the outputs using fuzzy sets that are easy to design. The final result is a weighted-up value for the certainty of existence of objects, which is called $c_{AF(x)}$. The following paragraphs describe how the fuzzy controller has been designed.

1) *Data Inputs*: The fuzzy controller data inputs consist of the following sources of information.

Certainty of the existence of objects for each barrier. The certainty of the existence of an object is given by the previously calculated value (the first level of the data fusion architecture) for both US and IR barriers. In both cases, they represent the degree of confidence about the existence of object, taking values from zero (tracks free of objects) to one (an obstacle exists). Two fuzzy sets (F “Free” and O “Obstacle detection”) are defined to indicate the state of the link [see Fig. 12(a)].

Wind-speed measurement. Wind speed has been considered from 0 to 10.5 m/s, as shown in Fig. 12(b). A wind speed that is higher than 10.5 m/s produces turbulences, causing the coherence time to be under the emission time; therefore, the emission becomes unrecognizable for the receiver [10]. Three fuzzy sets (L, M, and H) are defined, and their limits are set in function of the above-commented turbulence influence on the US barrier.

Visibility conditions. The confidence level of the IR barrier is adjusted according to the visibility conditions. Visibility takes values from 50 km (for very clear days) to 50 m (dense fog). Three fuzzy sets are defined (DF, C, and VC), and their limits are experimentally adjusted by using the IR barrier performance [see Fig. 12(c)] [23].

2) *Data Outputs*: The fuzzy controller output is the modified certainty of existence of an object in the area under supervision, including the environmental effects $c_{AF(x)}$. As Fig. 13 depicts, three fuzzy sets are defined (F, O, and I). Its range takes values from zero (free of obstacles) to one (obstacle detection). The I fuzzy set is added to model the situation when the correlation values are very low (which means that obstacles can exist); however, the weather conditions invalidate the measurements (high wind speed or very low visibility).

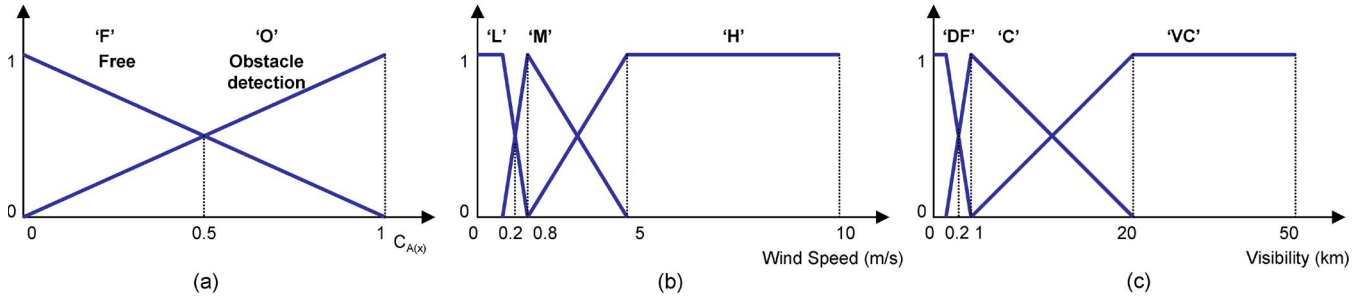


Fig. 12. Input fuzzy set membership functions. (a) Certainty of existence of objects $C_{A(x)}$ obtained in the previous stage. (b) Wind speed: L , low; M , medium; H high. (c) Visibility: DF , dense fog; C , clear; VC , very clear.

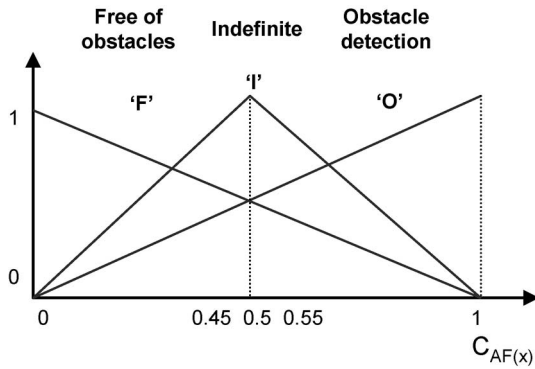


Fig. 13. Output fuzzy set membership functions.

3) *Rule definition and the defuzzification process:* Finally, a set of rules is necessary to transform the variables into a fuzzy result. The knowledge is typically represented in terms of if-then rules. An example is as follows: If A and B, then C. The if-part of the rule is called the *premise*, and the then-part is called the *consequent*. The truth value of the rule’s premise describes to what degree the rule applies in a given situation. The so-called *fuzzy inference mechanism* is used to determine the consequent fuzzy set based on the truth value of the premise (this is often called the *degree of fulfillment*). Consequent fuzzy sets of individual rules are then combined (*aggregated*) into a single fuzzy set. The resulting fuzzy set is converted (*defuzzified*) into a real (crisp) value, in this case indicating the fuzzy certainty of existence of objects $C_{AF(x)}$. Due to the fact that the source of false alarms in the proposed obstacle-detection scheme is mainly because of weather influence in the sensors, the objective of the fuzzy rules is to establish the logical relation between weather conditions and sensor measurements to decrease false alarms. The following premises should be considered to define the controller rules that fuse the information from both barriers.

- 1) If any barrier does not detect an object (the corresponding $C_{A(x)}$ is very low), the tracks are considered to be free of objects, independently of the other variables. This comes from the fact that the detection is based on the lack of a signal, which can be caused by several reasons: presence of an object (the one that causes alarm), a damaged sensor (emitter and/or receiver), weather conditions, etc. Nevertheless, the presence of a signal cannot be explained by any other factor apart from the obvious lack of objects.

TABLE II
APPLIED RULES WHEN AN OBJECT IS DETECTED BY BOTH BARRIERS
(‘O’ = OBSTACLE DETECTION ‘I’ = INDEFINITE)

	US barrier			
	IR barrier	‘O’		
‘O’	Wind speed	‘L’ Low	‘M’ Medium	‘H’ High
	‘DF’(Dense Fog)	‘O’	‘O’	‘I’
	‘C’ (Clear)	‘O’	‘O’	‘O’
	‘VC’(Very Clear)	‘O’	‘O’	‘O’

- 2) If an object is detected by both barriers ($C_{A(x)} > 0.5$) and the weather conditions are favorable, the fusion concludes that an object exists.
- 3) If an object is detected but there is dense fog, or it is windy, the lack of a signal can be caused by other circumstances as explained before and not only by the object; therefore, in this case, the output is undefined.

This reasoning produces a large set of rules that are summarized by applying the first premise. Table II only shows the applied rules when both barriers detect the existence of an object (second premise). According to Table II, if both barriers detect the presence of an obstacle and weather conditions are really bad (dense fog and high wind speed), it is impossible to conclude that an object exists. In this case, the fuzzy output is indefinite (“I”).

The operators that have to be defined in a fuzzy controller describe the operations between rules, in other words, the “and” connector, which is defined as the “minimum” operation, the “or” connector, which is defined as the “maximum” operation, and the “aggregation” of the different rules that are involved in the fusion process that is defined as the “maximum” operation. As was previously mentioned, since the controller is modeled as a Mamdani controller, a *defuzzification* process is necessary to obtain a quantifiable result in the fuzzy logic, as opposed to the Sugeno controller that uses numeric rules to obtain the output. There are several methods to transform the fuzzy outputs into a numerical value, which can be used by the next fusion step. The one used in this paper is the center-of-area (CoA) method [32], [33]. The CoA method calculates the center of gravity of

the final fuzzy control space, producing a result that is sensitive to all rules. The CoA is given by

$$C_{AF(x)} = \frac{\sum_{i=1}^s c_i v_i}{\sum_{i=1}^s v_i} \quad (8)$$

where c_i is the quantized value corresponding to the center of the output fuzzy sets, v_i is the membership value of the output fuzzy set, i is the index of the rule that is satisfied, s is the number of satisfied fuzzy rules, and $C_{AF(x)}$ is the crisp value of the output variable.

C. Third Level. The Dempster–Shafer Theory Application

After the values for the certainty of existence of objects are available for every area, they can be combined between consecutive areas $A_{(x)}$ and $A_{(x+1)}$ to obtain the certainty of existence of objects larger than $50 \times 50 \times 50$ cm. For this task, it is proposed to use the Dempster–Shafer evidential theory [30]. This probability-based data fusion classification algorithm is useful when the information sources contributing data cannot associate a 100% probability of certainty to their output decisions. In this theory, each information source associates a declaration or hypothesis with a probability mass, expressing the amount of support or belief directly attributed to the declaration, in other words, the certainty of the declaration. The probability masses for the decisions made by each information source are then combined by using Dempster’s rule of combination [28]. The hypothesis favored by the largest accumulation of evidence from all the information sources is selected as the most probable outcome of the fusion process. The Dempster–Shafer theory estimates how close the evidence is to forcing the truth of a hypothesis, rather than estimating how close the hypothesis is to being true [34].

In the application described in this paper, each area provides a number indicating the certainty of existence of objects $c_{AF(x)} \in [0, 1]$ obtained after the application of the fuzzy controller. If $c_{AF(x)}$ is considered as the probability mass of the certainty of existence of objects in the area $A_{(x)}$, a value $c_{o,x} \in [0, 1]$ can be obtained by applying directly Dempster’s rule [28], as shown in the following, representing the result of the fusion between the areas $A_{(x)}$ and $A_{(x+1)}$:

$$c_{o,x} = \frac{c_{AF(x)} \cdot c_{AF(x+1)}}{1 - (1 - c_{AF(x)}) \cdot c_{AF(x+1)} - (1 - c_{AF(x+1)}) \cdot c_{AF(x)}} \quad (9)$$

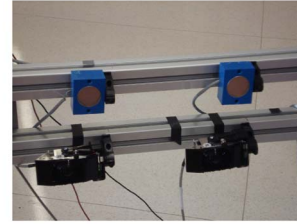
$c_{o,x}$ represents the accumulation of evidence from two consecutive areas: The higher the value of $c_{o,x}$, the higher the certainty of existence of objects larger than $50 \times 50 \times 50$ cm. However, if $c_{o,x}$ takes a value of 0.5, it means that there is a situation of uncertainty (it cannot be concluded if there exists a dangerous object). Values of $c_{o,x}$ lower than 0.5 mean that there is a certainty of absence of an object.

All the components $c_{o,x}$ can be arranged in a vector \mathbf{C}_O as shown in the following, with N_Z as the number of influence areas:

$$\mathbf{C}_O = [c_{o,1} \quad \cdots \quad c_{o,x} \quad \cdots \quad c_{o,(N_Z-1)}] \quad (10)$$



(a)



(b)

Fig. 14. Prototype of the multisensory barrier. (a) Emitting barrier. (b) Detail of US and IR receivers.

According to the number of consecutive components of vector \mathbf{C}_O higher than 0.5, it can be concluded how large the object is.

IV. RESULTS

To evaluate the feasibility of the proposed system and algorithms, a prototype of the multisensory barrier has been implemented (see Fig. 14), carrying out the encoding schemes for each sensor technology [17] and the validation of the existence of objects, as has been explained in Section III.

In Fig. 6, the real correlation outputs for an IR receiver are shown. Now, Fig. 15 shows the real correlation outputs but for a US receiver. In this case, there is a temporary object in front of emitter 3. As is shown, the detection of the object is carried out because of the lack of signal of emission 3 in the receiver (the correlation output for emission 3 is smaller than that for the fixed threshold). Simulated results have concluded that the encoding scheme can cope with signal-to-noise ratios that are lower than -10 dB [18].

Fig. 16 shows the scheme of a real example of detection, where there exist two objects: a small object and a dangerous one (larger than $50 \times 50 \times 50$ cm). For this test, the day was clear ($1 \text{ km} < \text{visibility} < 20 \text{ km}$), and the wind speed was low ($< 0.8 \text{ m/s}$). The validation of the existence of objects previously described has been carried out. First, the certainties of existence of objects in areas ($c_{A(x)}$) are computed for each barrier (first and second rows of the table in Fig. 16). Second, a certainty $c_{AF(x)}$ has been obtained after the application of the fuzzy controller (the third row of the table in Fig. 16). Finally, consecutive areas have been combined by using (10) to obtain the vector \mathbf{C}_o , containing the certainty of existence of objects that are larger than $50 \times 50 \times 50$ cm. In this case, five influence areas have been considered, where the result is $[0.97 \ 0.94 \ 0.25 \ 0.22]$. As the result shows, there is an object occupying three

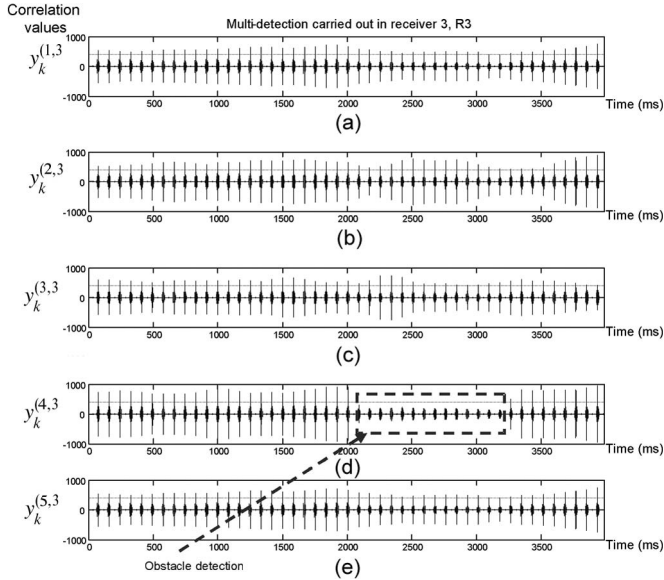
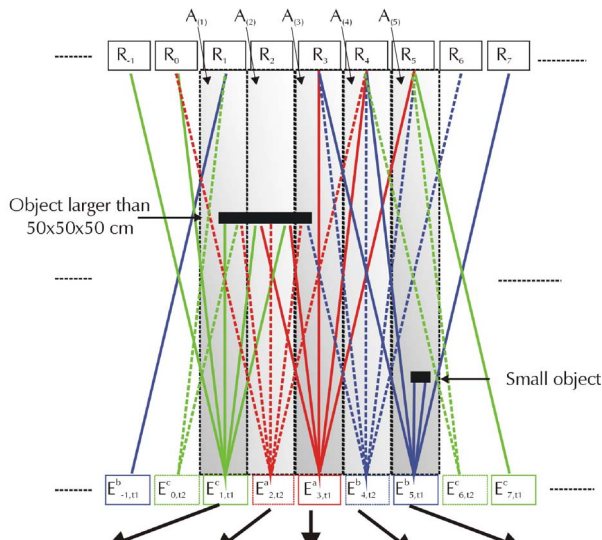


Fig. 15. Real correlation outputs obtained in a US receiver.

TABLE III
REAL DATA FOR THE INFLUENCE AREA 1 $A_{(1)}$

IR BARRIER $A_{(l)}$					
$l_{e,r} (e,r)$	z_k	\hat{y}_{k-1}	$\alpha_{e,r}$	$\rho_{e,r}$	$\sigma_{e,r}$
1,-1	ON	458.57	0.5	0.25	0
1,0	ON	485.02	0.5	0.5	0
2,0	ON	458.57	0.5	0.5	0
-1,1	ON	458.57	0.5	0.25	0
0,1	ON	485.02	0.5	0.5	0
1,1	OFF	511.57	0.5	1	0.5
2,1	OFF	485.02	0.5	0.5	0.25
3,1	OFF	458.57	0.5	0.25	0.12
0,2	OFF	458.57	0.5	0.5	0.25
1,2	OFF	485.02	0.5	0.5	0.25
1,3	OFF	458.57	0.5	0.25	0.12
US BARRIER $A_{(l)}$					
$l_{e,r} (e,r)$	z_k	\hat{y}_{k-1}	$\alpha_{e,r}$	$\rho_{e,r}$	$\sigma_{e,r}$
1,-1	ON	458.51	0.5	0.25	0
1,0	ON	464.08	0.5	0.5	0
2,0	ON	458.51	0.5	0.5	0
-1,1	ON	458.51	0.5	0.25	0
0,1	ON	464.08	0.5	0.5	0
1,1	OFF	464.08	0.5	1	0.52
2,1	OFF	464.08	0.5	0.5	0.26
3,1	OFF	458.51	0.5	0.25	0.12
0,2	OFF	458.51	0.5	0.5	0.25
1,2	OFF	464.08	0.5	0.5	0.26
1,3	OFF	458.51	0.5	0.25	0.12



Influence Areas	$A_{(1)}$	$A_{(2)}$	$A_{(3)}$	$A_{(4)}$	$A_{(5)}$
IR Barrier	$C_{A_{(1)}}=0.84$	$C_{A_{(2)}}=0.93$	$C_{A_{(3)}}=0.67$	$C_{A_{(4)}}=0.12$	$C_{A_{(5)}}=0.6$
US Barrier	$C_{A_{(1)}}=0.85$	$C_{A_{(2)}}=0.94$	$C_{A_{(3)}}=0.69$	$C_{A_{(4)}}=0.12$	$C_{A_{(5)}}=0.64$
Fuzz.Contr.	$C_{AF_{(1)}}=0.79$	$C_{AF_{(2)}}=0.9$	$C_{AF_{(3)}}=0.64$	$C_{AF_{(4)}}=0.16$	$C_{AF_{(5)}}=0.6$
	$C_{o,1}=0.97$				
		$C_{o,2}=0.94$			
			$C_{o,3}=0.25$		
				$C_{o,4}=0.22$	

Fig. 16. Real test of the sensor data fusion.

consecutive areas, whereas the small object is filtered since only two links are interrupted. As an example, Table III shows the data obtained from the two barriers in the first influence area $A_{(1)}$. All the parameters that appear in Table III have been previously described in Section III-A. In this test, for both barriers, the minimum threshold $T_{H-\min}$ is fixed at 100, and the process gain G is 1024. The parameter G depends on the correlation scheme, and it represents the maximum correlation output that can be obtained in an ideal situation. The minimum

threshold has been empirically fixed by taking into account the value of G and the expected noise ($T_{H-\min} \approx 0, 1 \cdot G$).

The situation shown in Fig. 16 has been tested under different weather conditions. Due to the fact that some of them are difficult to obtain, they have been artificially forced. To assess the influence of wind, in addition to the use of fans, windy days were chosen for testing. For the reduction of visibility, according to the weather conditions [19], optical filters have been used to reduce the level of the signal in the IR receivers.

Table IV shows the results with dense fog (visibility < 100 m) and low wind speed (< 0.8 m/s), and Table V shows those in a clear day (visibility > 1 km) and high wind speed (> 5 m/s). As the results show, the system is working correctly if there is only one adverse situation: dense fog or high wind speed. The system has also been evaluated under extreme weather conditions (dense fog and high wind speed at the same time). The results are shown in Table VI. In this case, each barrier correctly detects the presence of objects; however, the fuzzy controller provides a result of the existence of objects ($C_{AF(x)}$) close to 0.5 (but lower than 0.5) in the areas where

TABLE IV
RESULTS OF THE REAL TEST WITH DENSE FOG (VISIBILITY < 100 m)
AND LOW WIND SPEED (< 0.8 m/s)

Influence Areas	$A_{(1)}$	$A_{(2)}$	$A_{(3)}$	$A_{(4)}$	$A_{(5)}$
IR Barrier	$c_{A(1)}=0.59$	$c_{A(2)}=0.73$	$c_{A(3)}=0.42$	$c_{A(4)}=0.06$	$c_{A(5)}=0.39$
US Barrier	$c_{A(1)}=0.85$	$c_{A(2)}=0.94$	$c_{A(3)}=0.69$	$c_{A(4)}=0.12$	$c_{A(5)}=0.64$
Fuzzy Controller	$c_{AF(1)}=0.57$	$c_{AF(2)}=0.69$	$c_{AF(3)}=0.43$	$c_{AF(4)}=0.08$	$c_{AF(5)}=0.41$
		$c_{o,1}=0.76$			
			$c_{o,2}=0.64$		
				$c_{o,3}=0.06$	
					$c_{o,4}=0.06$

TABLE V
RESULTS OF THE REAL TEST IN A CLEAR DAY (VISIBILITY > 1 km)
AND HIGH WIND SPEED (> 5 m/s)

Influence Areas	$A_{(1)}$	$A_{(2)}$	$A_{(3)}$	$A_{(4)}$	$A_{(5)}$
IR Barrier	$c_{A(1)}=0.83$	$c_{A(2)}=0.93$	$c_{A(3)}=0.67$	$c_{A(4)}=0.12$	$c_{A(5)}=0.62$
US Barrier	$c_{A(1)}=0.60$	$c_{A(2)}=0.74$	$c_{A(3)}=0.44$	$c_{A(4)}=0.06$	$c_{A(5)}=0.38$
Fuzzy Controller	$c_{AF(1)}=0.58$	$c_{AF(2)}=0.70$	$c_{AF(3)}=0.45$	$c_{AF(4)}=0.09$	$c_{AF(5)}=0.40$
		$c_{o,1}=0.77$			
			$c_{o,2}=0.67$		
				$c_{o,3}=0.08$	
					$c_{o,4}=0.06$

TABLE VI
RESULTS OF THE REAL TEST WITH DENSE FOG (VISIBILITY < 100 m)
AND HIGH WIND SPEED (> 5 m/s)

Influence Areas	$A_{(1)}$	$A_{(2)}$	$A_{(3)}$	$A_{(4)}$	$A_{(5)}$
IR Barrier	$c_{A(1)}=0.59$	$c_{A(2)}=0.73$	$c_{A(3)}=0.42$	$c_{A(4)}=0.06$	$c_{A(5)}=0.39$
US Barrier	$c_{A(1)}=0.60$	$c_{A(2)}=0.74$	$c_{A(3)}=0.44$	$c_{A(4)}=0.06$	$c_{A(5)}=0.38$
Fuzzy Controller	$c_{AF(1)}=0.46$	$c_{AF(2)}=0.48$	$c_{AF(3)}=0.39$	$c_{AF(4)}=0.08$	$c_{AF(5)}=0.36$
		$c_{o,1}=0.44$			
			$c_{o,2}=0.37$		
				$c_{o,3}=0.05$	
					$c_{o,4}=0.05$

objects exist. The reason is that weather conditions are so bad that the level of confidence of the data provided by the barriers is very low. In such situations, it is complicated to reliably conclude if objects exist. It is important to consider that this situation (high wind speed and dense fog at the same time) is difficult to find in real life.

Fig. 17 shows another real test. Only IR barrier links are represented. In this case, there are four *small objects* that are randomly interrupting several links in both barriers—links (2, 1), (1, 3), (3, 3), (3, 5), and (5, 6); IR emitter 4 is not working (simulating that it is damaged); the day was clear (visibility > 1 km), and the wind speed was medium (0.2 m/s < wind speed < 5 m/s). Table VII shows the results obtained after applying the algorithms.

As the results show, for the IR barrier, there exist objects (mainly because one emitter is not working). However, the

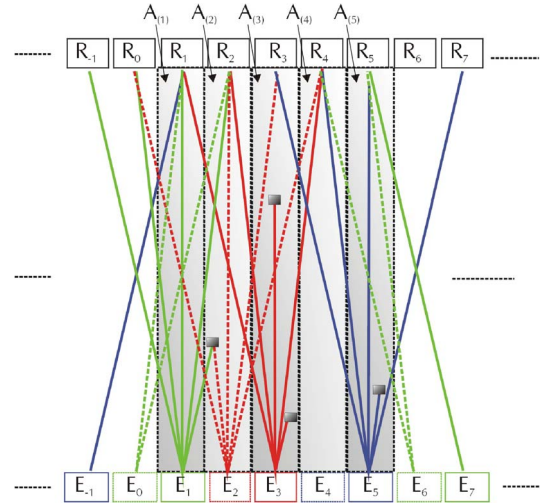


Fig. 17. Real test with small objects and a damaged emitter.

TABLE VII
RESULTS OF THE REAL TEST SHOWN IN FIG. 17

Influence Areas	$A_{(1)}$	$A_{(2)}$	$A_{(3)}$	$A_{(4)}$	$A_{(5)}$
IR Barrier	$c_{A(1)}=0.34$	$c_{A(2)}=0.50$	$c_{A(3)}=0.78$	$c_{A(4)}=0.83$	$c_{A(5)}=0.63$
US Barrier	$c_{A(1)}=0.26$	$c_{A(2)}=0.33$	$c_{A(3)}=0.48$	$c_{A(4)}=0.18$	$c_{A(5)}=0.26$
Fuzzy Controller	$c_{AF(1)}=0.30$	$c_{AF(2)}=0.36$	$c_{AF(3)}=0.47$	$c_{AF(4)}=0.22$	$c_{AF(5)}=0.30$
		$c_{o,1}=0.20$			
			$c_{o,2}=0.34$		
				$c_{o,3}=0.20$	
					$c_{o,4}=0.11$

algorithm filters those situations where there are several small objects, or a sensor in a barrier is off due to the fact that the corresponding sensor in the other barrier is working properly. If two sensors, i.e., one in each barrier, occupying the same position are simultaneously off, the algorithm considers that there is a *small object* since only one influence area is affected, but the alarm is not generated.

It is important to consider that the results shown correspond to one time instant. According to the encoding scheme, every 102.4 ms, the barriers provide a set of data. Railway Regulations required a scan time of 500 ms, and if an obstacle is inside the detection area for more than 3 s, an alarm must be generated. In that time, this system can give almost 30 measurements about the state of the tracks using two different technologies. Therefore, reliable information can be provided for safe train circulation.

V. CONCLUSION

A proposal of a multisensory system for obstacle detection on railways has been proposed, based on the complementary use of IR and US barriers, achieving high reliability. In this paper, apart from the use of two different sensor technologies, the reliability of the detection system has been increased due to

the following reasons. First, a robust encoding scheme based on mutually orthogonal complementary sets of sequences has been implemented. It provides multiemission and multireception, avoids interferences among the emissions, and can cope with low signal-to-noise ratios. Second, a fuzzy controller has been included to combine the information given by the two sensors (IR and US). It generates a value for the certainty of the existence of objects considering some external agents, such as visibility and wind speed that can affect the sensor measurements. This controller distinguishes situations where a barrier is not properly working from the existence of objects. Finally, the fusion of this information by means of the Dempster–Shafer evidential theory has been proposed to obtain a certainty value for the existence of objects posing a risk to railway traffic (larger than $50 \times 50 \times 50$ cm).

Another important aspect of the multisensory system presented here is its spatial redundancy. The detection area is a net of links for each barrier, and if an object that is greater than $50 \times 50 \times 50$ cm is detected, at least ten links are simultaneously interrupted (in each barrier). To distinguish situations where random interruptions of the links happen (such as in the case of small animals, flying leaves, an out-of-order sensor, etc.) from the existence of objects, the detection area has been divided into influence areas, fusing the information by means of the evidential theory to finally obtain a reliable value for the existence of objects.

A prototype of the multisensory barrier has been developed to show the feasibility of the proposal, and the experimental results demonstrate its reliability.

REFERENCES

- [1] M. Arai, "Railway safety for the 21st century," *Jpn. Railway Transp. Rev.*, vol. 36, pp. 42–47, Sep. 2003.
- [2] P. Bon and C. Cassir, *Overview of National and European projects European Commission, Fifth Framework Programme SAMNET Thematic Network*, Feb. 12, 2004, INRETS; Techn. Univ. Dresden, Dresden, Germany, Railway Safety Management.
- [3] *REOST Project Description*, 2004. [Online]. Available: <http://spt.dibe.unige.it/ISIP/reost/projectdescription.html>
- [4] M. Ghazel, "Using stochastic Petri nets for level-crossing collision risk assessment," *IEEE Trans. Intell. Transp. Syst.*, vol. 10, no. 4, pp. 668–677, Dec. 2009, Digital Object Identifier 10.1109/TITS.2009.2026310.
- [5] Laseroptronix Co., [Online]. Available: <http://www.laseroptronix.com/rail/>
- [6] Canadian Pacific Railway, *Railway Rockfall Electromagnetic Field Disturbance Sensing System Development and Test Results*, Oct. 2002.
- [7] Cerberus, 2000. [Online]. Available: <http://www.buildingtechnologies.siemens.com>
- [8] K. Krishnaswami and M. Tilleman, "Off the line-of-sight laser radar," *Appl. Opt.*, vol. 37, no. 3, pp. 565–572, Jan. 1998.
- [9] H. Weichel, *Laser Beam Propagation in The Atmosphere*. Bellingham, WA: SPIE, 1990, ser. Tutorial texts in optical engineering.
- [10] F. J. Álvarez, J. Ureña, A. Hernández, M. Mazo, J. J. García, and A. Jiménez, "Influence of atmospheric refraction on the performance of an outdoor ultrasonic pulse compression system," *Appl. Acoust.*, vol. 69, no. 11, pp. 994–1002, Sep. 2007.
- [11] N. V. Murali, C. Chandramouli, and V. Agarwal, "A cost-effective ultrasonic sensor-based driver-assistance system for congested traffic conditions," *IEEE Trans. Intell. Transp. Syst.*, vol. 10, no. 3, pp. 486–498, Sep. 2009.
- [12] C. Caraffi, S. Cattani, and P. Grisleri, "Off-road path and obstacle detection using decision networks and stereo vision," *IEEE Trans. Intell. Transp. Syst.*, vol. 8, no. 4, pp. 607–618, Dec. 2007.
- [13] T. Kato, Y. Ninomiya, and I. Masaki, "An obstacle detection method by fusion of radar and motion stereo," *IEEE Trans. Intell. Transp. Syst.*, vol. 3, no. 3, pp. 182–188, Sep. 2002.
- [14] Y. Ruichek, "Multilevel- and neural-network-based stereo-matching method for real-time obstacle detection using linear cameras," *IEEE Trans. Intell. Transp. Syst.*, vol. 6, no. 1, pp. 54–62, Mar. 2005.
- [15] "System for falling obstacle detection on the railway," Technical and Functional Requirements. GIF, 2001 (in Spanish).
- [16] Y. Chen, Q.-J. Kong, Y. Liu, and Z. Li, "An approach to urban traffic state estimation by fusing multisource information," *IEEE Trans. Intell. Transp. Syst.*, vol. 10, no. 3, pp. 499–511, Sep. 2009.
- [17] M. J. Díaz, J. J. García, Á. Hernández, C. Losada, and E. García, "Advanced multisensorial barrier for obstacle detection," in *Proc. IEEE Int. Symp. WISP*, Madrid, Spain, 2007, pp. 549–554.
- [18] J. J. García, C. Losada, F. Espinosa, J. Ureña, Á. Hernández, M. Mazo, C. de Marziani, A. Jiménez, E. Bueno, and F. Álvarez, "Dedicated smart IR barrier for obstacle detection in railway," in *Proc. IEEE IECON*, Raleigh, NC, 2005, pp. 439–444.
- [19] J. J. García, C. Losada, F. Espinosa, J. Ureña, Á. Hernández, M. Mazo, C. de Marziani, A. Jiménez, F. Álvarez, and J. A. Jiménez, "Optimal estimation techniques to reduce false alarms in railway obstacle detection," in *Proc. IEEE ICIT*, Hong Kong, 2005, pp. 459–464.
- [20] C. C. Tseng and C. L. Liu, "Complementary sets of sequences," *IEEE Trans. Inf. Theory*, vol. IT-18, no. 5, pp. 644–652, Sep. 1972.
- [21] A. Chow, "Performance of spreading Codes for direct sequence code division multiple access (DS-CDMA)," Stanford Univ., Stanford, CA, Dec. 5, 2003.
- [22] C. De Marziani, J. Ureña, Á. Hernández, M. Mazo, F. J. Álvarez, J. J. García, and P. Donato, "Modular architecture for efficient generation and correlation of complementary set of sequences," *IEEE Trans. Signal Process.*, vol. 55, no. 5, pp. 2323–2337, May 2007.
- [23] S. Bloom, E. Korevaar, J. Schuster, and H. Willebrand, "Understanding the performance of free-space optics [Invited]," *J. Opt. Netw.*, vol. 2, no. 6, pp. 178–200, Jun. 2003.
- [24] N. Hautiere, R. Labayrade, and D. Aubert, "Real-time disparity contrast combination for onboard estimation of the visibility distance," *IEEE Trans. Intell. Transp. Syst.*, vol. 7, no. 2, pp. 201–212, Jun. 2006.
- [25] D. Simon, "From here to infinity," *Embedded Systems Programming Magazine*, pp. 2–9, Jul. 2000.
- [26] X. Shen and L. Deng, "Game theory approach to discrete H_∞ to filter design," *IEEE Trans. Signal Process.*, vol. 45, no. 4, pp. 1092–1095, Apr. 1997.
- [27] U. Shaked and Y. Theodor, " H_∞ optimal estimation: A tutorial," in *Proc. IEEE 31st Conf. Decision Control*, Tucson, AZ, Dec. 1992, pp. 2278–2286.
- [28] L. A. Klein, *Data and Sensor Fusion: A Tool for Information Assessment and Decision Making*. Bellingham, WA: SPIE, 2004.
- [29] H. Ying, *Fuzzy Control and Modeling: Analytical Foundations and Applications*. New York: Wiley-IEEE Press, Aug. 2000.
- [30] G. Shafer, *A Mathematical Theory of Evidence*. Princeton, NJ: Princeton Univ. Press, 1976.
- [31] E. H. Mamdani and S. Assilian, "An experiment in linguistic synthesis with a fuzzy logic controller," *Int. J. Man-Mach. Stud.*, vol. 7, no. 1, pp. 1–13, Jan. 1975.
- [32] J. E. Naranjo, C. Gonzalez, R. Garcia, and T. de Pedro, "Lane-change fuzzy control in autonomous vehicles for the overtaking maneuver," *IEEE Trans. Intell. Transp. Syst.*, vol. 9, no. 3, pp. 438–450, Sep. 2008.
- [33] K. M. Passino and S. Yurkovich, *Fuzzy Control*. Reading, MA: Addison-Wesley, 1998.
- [34] J. Pearl, *Probabilistic Reasoning in Intelligent Systems: Networks of Plausible Inference*. San Mateo, CA: Morgan Kaufmann, 1988.



J. Jesús García (M'06) received the B.Sc. degree in electronic engineering and the Ph.D. degree with distinction from the University of Alcalá, Madrid, Spain, in 1992 and 2006, respectively, and the M.Sc. degree from the Polytechnic University of Valencia, Valencia, Spain, in 1999.

He is currently an Associate Professor of digital and analog electronics with the Department of Electronics, University of Alcalá. He has worked on several public and private research projects related to digital control and sensory systems, mainly applied to the railway transport system. He has authored or coauthored more than 75 publications in these fields. His research areas include multisensor integration, local positioning systems, and sensory systems for railway safety.



Jesús Ureña (M'06) was born in Jaén, Spain, in 1964. He received the B.S. degree in electronics engineering and the M.S. degree in telecommunications engineering from the Polytechnical University of Madrid, Madrid, Spain, in 1986 and 1992, respectively, and the Ph.D. degree in telecommunications from the University of Alcalá, Madrid, in 1998.

Since 1986, he has been with the Department of Electronics, University of Alcalá, where he is currently an Associate Professor. From 1993 to 1997, he was the Head of the department. He has collaborated on several educational and research projects in the area of electronic control and sensorial systems for mobile robots and wheelchairs and in the area of electronic distributed systems for railways. His current research interests include the areas of low-level ultrasonic signal processing, local positioning systems, and sensory systems for railway safety.



Álvaro Hernández (M'06) received the electronic engineering degree from the University of Alcalá, Madrid, Spain, in 1998 and the Ph.D. degree from the University of Alcalá and from the Blaise Pascal University, Clermont-Ferrand, France, in 2003.

He is currently an Associate Professor of electronic design with the Department of Electronics, University of Alcalá. His research areas include multisensor integration, electronic systems for mobile robots, digital systems, embedded systems, and computing architectures.



Manuel Mazo (M'91) received the Ph.D. degree in telecommunications and the M.Sc. degree in engineering degree in telecommunications from the Polytechnical University of Madrid, Madrid, Spain, in 1982 and 1988, respectively.

He is currently a Professor with the Department of Electronics, University of Alcalá, Madrid. During his career, he has collaborated on several research projects, and he has published more than 100 technical papers. His research interests include electronics control, intelligent sensors (ultrasonic, infrared, and artificial vision), robot sensing and perception, intelligent spaces, electronics systems for railway safety, and wheelchairs for physically disabled people.



José Antonio Jiménez received the electronic telecommunication engineering degree from the University of Valencia, Valencia, Spain, in 1996 and the Ph.D. degree from the University of Alcalá, Madrid, Spain, in 2004.

He is currently an Associate Professor of instrumentation electronics with the Department of Electronics, University of Alcalá. His research areas include multisensor integration, sensorial systems applied to robotics, instrumentation, and electronic systems for mobile robots.



Fernando J. Álvarez received the Physics degree from the University of Sevilla, Sevilla, Spain, in 1998 and the Ph.D. degree in electronics from the University of Alcalá, Madrid, Spain, in 2006.

He is currently an Associate Professor of control engineering and digital electronics with the Department of Electrical Engineering, Electronics, and Automatics, University of Extremadura, Badajoz, Spain. His research areas of interest include outdoor acoustics, ultrasonic signal processing, and airborne sonar systems.



Carlos De Marziani received the electronics engineering degree from the University of Patagonia San Juan Bosco, Patagonia, Argentina, in 2001 and the Ph.D. degree from the University of Alcalá, Madrid, Spain, in 2007.

He is currently a Professor of digital systems with the Department of Electronics, University of Patagonia San Juan Bosco, as well as an Assistant Researcher with the National Council on Scientific and Technical Research, Buenos Aires, Argentina (Consejo Nacional de Investigaciones Científicas y Técnicas). His research areas include sensor networks, multisensor integration, electronic systems for mobile robots, and digital systems.



Ana Jiménez received the physics degree from the Complutense University of Madrid, Madrid, Spain, in 1995 and the degree in materials engineering and the Ph.D. degree from the Polytechnic University of Madrid, Madrid, in 1999 and 2003, respectively.

She has worked in molecular beam epitaxy growth, fabrication, and characterization of AlGaIn/GaN heterostructures for electronic applications. In January 2004, she joined the Department of Electrical Engineering, University of Alcalá, Madrid, as an Assistant Professor. Her current research interests are focused on ultrasonic transducers, the design of acquisition, and analysis and processing systems for ultrasonic transducers for mobile robots.



M. Jesús Díaz received the B.S. degree in electrical engineering and the M.S. degree in electronics engineering in 2005 and 2007, respectively, from the University of Alcalá, Madrid, Spain, where she is currently working toward the Ph.D. degree in power electronics.

From 2005 to 2008, she was a Researcher with the Department of Electronics, University of Alcalá. Her research interests are focused on signal processing using field programmable gate arrays, control engineering, and sensory systems for railway safety.



Cristina Losada received the B.S. and M.S. degrees in electrical and electronic engineering in 2004 from the University of Alcalá, Madrid, Spain, where she is currently working toward the Ph.D. degree with the Department of Electronics.

Her research interests are focused on intelligent spaces and sensory systems.



Enrique García was born in Madrid, Spain, in 1986. He received the B.S. degree in industrial electronics engineering and the M.Sc. degree in advanced electronics systems in 2007 and 2009, respectively, from the University of Alcalá, Madrid, where he is currently working toward the Ph.D. degree in electronics with the Department of Electronics.

His main research interests include the areas of signal processing, sensor systems, and local positioning systems.